

THE CORRELATED k -DISTRIBUTION TECHNIQUE AS APPLIED TO THE AVHRR CHANNELS

DAVID P. KRATZ

Atmospheric Sciences Division, NASA Langley Research Center, Hampton, VA 23681-0001, U.S.A.

(Received 27 September 1994)

Abstract—Correlated k -distributions have been created to account for the molecular absorption found in the spectral ranges of the five Advanced Very High Resolution Radiometer (AVHRR) satellite channels. The production of the k -distributions was based upon an exponential-sum fitting of transmissions (ESFT) technique which was applied to reference line-by-line absorptance calculations. To account for the overlap of spectral features from different molecular species, the present routines made use of the multiplication transmissivity property which allows for considerable flexibility, especially when altering relative mixing ratios of the various molecular species. To determine the accuracy of the correlated k -distribution technique as compared to the line-by-line procedure, atmospheric flux and heating rate calculations were run for a wide variety of atmospheric conditions. For the atmospheric conditions taken into consideration, the correlated k -distribution technique has yielded results within about 0.5% for both the cases where the satellite spectral response functions were applied and where they were not. The correlated k -distribution's principal advantage is that it can be incorporated directly into multiple scattering routines that consider scattering as well as absorption by clouds and aerosol particles.

1. INTRODUCTION

Establishing the radiative effect of molecular absorption in the atmosphere is important in determining radiances not only for clear sky conditions but also for sky conditions with the presence of clouds and aerosol layers. Without an accurate accounting of molecular absorption, interpreting the meaning of retrieved satellite radiances could be fraught with errors.

Numerous modeling techniques are available to account for the observed absorption of electromagnetic radiation by the molecules which are present in planetary atmospheres. The line-by-line procedure is very precise and has an accuracy which is limited only by the extent of our knowledge of the interactions of matter with energy. Such precision, however, is only obtained at the cost of very intensive routines which are not practical in production calculations. To overcome the computational burden of the line-by-line procedure, narrowband^{1,2} and broadband^{3,4} techniques have been devised. While these band models can be made arbitrarily accurate for a homogeneous (constant temperature, pressure, etc.) atmospheres, they require a scaling procedure to account for the nonhomogeneity found in realistic atmospheres.⁵⁻⁸ In essence, the scaling procedure transforms the nonhomogeneous pathlength found in a realistic atmosphere into an equivalent homogeneous pathlength. While entirely satisfactory for the case where only absorption is present, such a transformation is not acceptable for cases where scattering is involved.⁹ Nevertheless, a technique known as the correlated k -distribution^{7,9-12} has been devised which can accurately and efficiently calculate molecular absorption for a nonhomogeneous path without the need to resort to a scaling approximation.

It is therefore the purpose of this report to examine the atmospheric molecular absorption found in the Advanced Very High Resolution Radiometer (AVHRR) satellite channels and to create reasonably straightforward yet accurate parameterizations of this absorption. To accomplish this goal, the present study employs a line-by-line procedure to create the correlated k -distributions. This line-by-line procedure is reviewed in the second section. The third section is a review of the philosophy and methodology behind the correlated k -distribution. The fourth section is a presentation of the construction of the correlated k -distributions for the five AVHRR satellite channels. Once constructed, it is necessary to test the accuracy of the correlated k -routines against

the line-by-line procedure. The fifth section is a comparison of the flux and heating rate results from the correlated k -routines to the results of the line-by-line procedure. Some concluding remarks are then presented in the sixth section.

2. THE LINE-BY-LINE PROCEDURE

The line-by-line, or monochromatic, procedure is currently the most detailed approach for theoretically obtaining the absorption coefficient of a particular molecular species. The absorption coefficient may be expressed as:

$$k_{\omega}(p, \theta) = \sum_i S_i(\theta) f_{i,\omega}(p, \theta), \quad (1)$$

where ω is the wavenumber, p is the pressure, θ is the temperature, $S_i(\theta)$ is the intensity of the i th line, and $f_{i,\omega}(p, \theta)$ is the line shape factor. The temperature dependence of the line intensities, as obtained from quantum theory, is given by:

$$S(\theta) = S_0 \frac{Z_{\omega}(\theta_0)}{Z_{\omega}(\theta)} \left(\frac{\theta_0}{\theta} \right)^m \exp \left[\frac{hc}{b_k} E'' \left(\frac{1}{\theta_0} - \frac{1}{\theta} \right) \right], \quad (2)$$

where h is Planck's constant, c is the speed of light, b_k is Boltzmann's constant, E'' is the energy of the lower state, Z_{ω} is the vibrational partition function, S_0 is the line intensity at $\theta_0 = 296$ K, and m is the exponent for the temperature dependence of the rotational partition function. The value of m is taken to be 1.0 for the linear molecules CO_2 and O_2 , and 1.5 for both the asymmetric top molecule H_2O and the spherical top molecule CH_4 . For conditions encountered in the present calculations, the contribution to the temperature dependence of the line intensity by stimulated emission is quite small ($< 1\%$). Moreover, inclusion of stimulated emission results in a substantial increase in the computational burden; therefore, stimulated emission will not be considered. The pressure and temperature dependence of the air-broadened Lorentz halfwidth is given by:

$$\gamma_i = \gamma_i^0 \left(\frac{p}{p_0} \right) \left(\frac{\theta_0}{\theta} \right)^n, \quad (3)$$

for each line, where γ_i^0 is the halfwidth of the i th line and $p_0 = 1$ atm. The exponent n of the temperature dependence of the Lorentz halfwidth is taken to be 0.77 for CO_2 , 0.50 for O_2 , 0.62 for H_2O , and 1.00 for CH_4 .¹³ For present purposes, the line shape factor is determined by utilizing Schreier's¹⁴ vectorized formulation of Humlíček's¹⁵ Voigt algorithm. Each Voigt line is taken to have a line cutoff of 256 times the Lorentz halfwidth or five times the Doppler halfwidth, whichever is greater. Such a cutoff is incorporated both for computational efficiency and as an effective parameterization of the sub-Lorentzian nature of the far line wings.^{16,17} It should be noted that for cases where the atmospheric pressure is very low, a line cutoff of 256 times the Lorentz halfwidth may be comparable to or smaller than the Doppler halfwidth.⁹ Thus, to ensure that the line cutoff is greater than the Doppler halfwidth, the cutoff criteria explicitly take into account the size of the Doppler halfwidth. As a result of the current cutoff criteria, roughly 0.25% of the integrated intensity of the Voigt line is not included in the calculation.

The line locations, intensities, air-broadened Lorentz halfwidths, and lower state energies were taken from the 1992 version of the Air Force Geophysics Laboratory (AFGL) HITRAN database.¹³ The line absorption considered in this study included the contributions attributed to H_2O for all five of the AVHRR channels, CO_2 for AVHRR channel 4, CH_4 for AVHRR channel 3, and O_2 for AVHRR channels 1 and 2. The absorption coefficients were computed with spectral resolutions of 0.01 cm^{-1} for AVHRR channels 1 and 2, and 0.005 cm^{-1} for AVHRR channels 3, 4 and 5. As noted by Chou and Kouvaris¹⁷ and Chou,¹⁸ the line-by-line procedure need not resolve individual absorption lines in order to yield highly accurate radiative transfer calculations. It is, however, important to determine the spectral resolution necessary to yield accurate and stable line-by-line calculations. The spectral resolutions chosen for the present study, while somewhat more conservative than those suggested by Chou and Kouvaris,¹⁷ ensure accurate absorption calculations well into the stratosphere.

Absorption by H_2O in AVHRR channels 4 and 5 has been attributed not only to individual lines, but also to a continuum. The nature of this water continuum is a controversial topic.^{19,20} In view

of the prevailing controversy, an acceptable means of accounting for the effect of the water vapor continuum absorption within the calculations is the application of the empirical formula of Roberts et al.²¹ which is frequently employed by climate modelers.²² As per the suggestion of Ridgway et al.,²³ the current calculations will only take into consideration the self-broadened e -type contribution.

In addition, a relatively weak absorption by the O₃ Chappuis band covers much of the spectral range of AVHRR channel 2 and all of the spectral range of AVHRR channel 1.^{7,24–26} Characterized by an extremely dense line structure, the absorption due to the Chappuis bands is essentially in the smeared-out line structure limit²⁷ for typical atmospheric pressures and temperatures. Thus, it is not surprising that the Chappuis bands are absent from the AFGL HITRAN database.¹³ Nevertheless, moderate resolutions, 5 cm⁻¹ throughout the AVHRR bands, O₃ cross sections for the Chappuis are available from Table 7.4 of WMO report No. 16.²⁵ It has been noted^{7,28} that the temperature dependence of the absorption coefficients for the Chappuis bands is negligible. Lacis and Hansen²⁸ have also indicated that the Chappuis bands are insensitive to pressure variations, and have further demonstrated that the absorption in the Chappuis bands is nearly proportional to the O₃ abundance. While not ideal, the WMO cross sections for the Chappuis bands should prove sufficient for applications to atmospheric modeling.²⁵

Since the radiative process of absorption and emission (and scattering) are wavenumber coherent,⁹ the line-by-line procedure may be integrated over a given spectral interval $\Delta\omega$, for a pathlength u , to yield the spectral-mean transmission $T_{\Delta\omega}(u, p, \theta)$, which may be expressed as:

$$T_{\Delta\omega}(u, p, \theta) = \int_{\Delta\omega} \exp\left[-k_{\omega}(p, \theta)u\right] \frac{d\omega}{\Delta\omega}. \quad (4)$$

The results of the line-by-line calculations can be given very precisely and with accuracies limited only to the extent of our knowledge of the physical processes involved and of the various input parameters utilized in the calculations. The line-by-line procedure, however, requires a substantial amount of computer processing time. Considering the large number of physical processes which must be taken into account, dedicating so much time to molecular absorption is not practical in production calculations. Nevertheless, the line-by-line procedure is extremely useful as a tool to parameterize the observed molecular absorption and as a reference against which to compare the various less-detailed models.

3. THE CORRELATED k -PROCEDURE AND EXPONENTIAL-SUM FITTING

Under conditions prevalent in the Earth's atmosphere, the spectra of most absorbing gases are characterized by highly complex distributions of absorption coefficient $k_{\omega}(p, \theta)$, with wavenumber ω [see, e.g., Fig. 1(a)]. As noted in the previous section, the line-by-line procedure resorts to retracing the relation between absorption coefficient and wavenumber with sufficient spectral resolution to accurately reproduce the spectrum of absorption coefficients. An examination of the relationship of the absorption coefficients vs wavenumber, however, reveals that similar values of $k(p, \theta)$ reoccur frequently. Computational efficiency can, therefore, be dramatically improved by substituting the integration over wavenumber by an integration over $h(k)$, the probability distribution function of the absorption coefficient. The function $h(k)$ is so constructed that $h(k) dk$ defines the fraction of $\Delta\omega$ contained between the absorption coefficient values of k and $k + dk$. For a homogeneous pathlength (constant pressure and temperature) and a wavenumber interval sufficiently small that the variations in the Planck function may be neglected, the spectral-mean transmission should be dependent upon $h(k)$ while being independent of the wavenumber ordering $k(p, \theta)$. This gives rise to the concept of the k -distribution method.^{29–32} Allowing the magnitude range of the absorption coefficients to extend from 0 to ∞ , the spectral-mean transmission from Eq. (4) may be rewritten as:

$$T_{\Delta\omega}(u, p, \theta) = \int_0^{\infty} \exp[-k(p, \theta)u] h(k) dk, \quad (5)$$

where $h(k)$ is normalized to 1 over the range of $k(p, \theta)$. It has been found,^{9,11,12} however, that it is more practical to express the k -distribution in terms of the cumulative probability function:

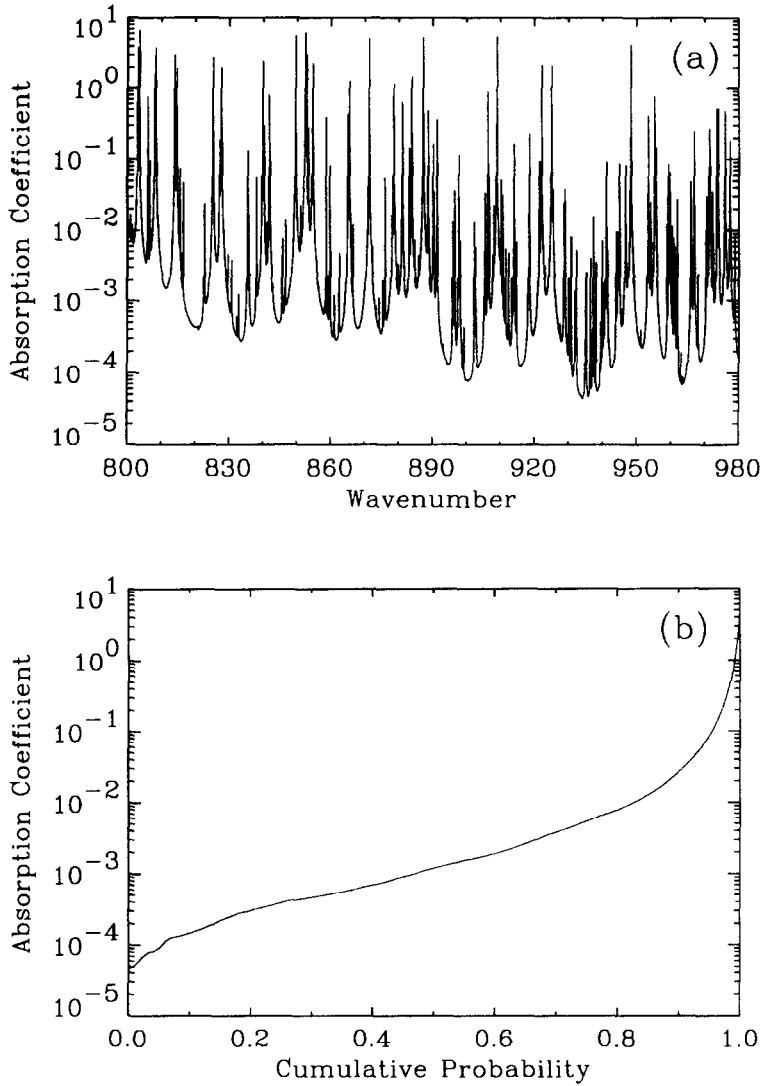


Fig. 1. Absorption coefficient, k , with units [$\text{cm}^{-1}/(\text{g}/\text{cm}^2)$] as a function of (a) wavenumber and (b) cumulative probability for H_2O line absorption at a pressure of 500 hPa and temperature of 250 K for the wavenumber interval of 800–980 cm^{-1} .

$$g(k) = \int_0^k h(k) dk, \quad (6)$$

and its inverse:

$$k(g) = g^{-1}(k). \quad (7)$$

By definition k is a monotonically increasing and smooth function in $g(k)$ space and vice versa⁹ [see, e.g., Fig. 1(b)]. Thus, the spectral-mean transmission may be rewritten as:

$$T_{\Delta\omega}(u, p, \theta) = \int_0^1 \exp[-k_g(p, \theta)u] dk, \quad (8)$$

As with other band model procedures, the k -distribution method relies upon a scaling procedure⁸ to account for nonhomogeneity in the atmosphere. Scaling procedures, however, may lead to substantial deviations as compared to reference line-by-line calculations.⁹ To avoid these potential errors, Lacis et al¹⁰ proposed extending the k -distribution to nonhomogeneous paths by assuming that for any pressure and temperature encountered in the atmosphere, any particular absorption coefficient will always be found to have the same cumulative probability. Thus, the location in

cumulative probability space of any absorption coefficient at any given pressure or temperature will be correlated with that of the absorption coefficient at a specified reference pressure and temperature. This leads to the concept of the correlated k -distribution.

Fu and Liou⁹ have investigated the physical and mathematical conditions under which the correlated k -distribution method is applicable. Their analyses have demonstrated that the correlated k -distribution technique is exact for the following cases: single lines, periodic lines of equal intensity, and lines in both the strong and weak line limits. For the strong and weak line limits, Goody et al²¹ have further presented formal proofs of the validity of the correlated k -distribution. In addition, Fu and Liou⁹ have investigated the assumption of correlation for realistic absorption spectra where deviations occur because of temperature dependences in line strengths and lower state energies, and because of pressure and temperature dependences in half-widths and line overlap. They have demonstrated conclusively that, despite the observed deviations, the assumption of correlation is sufficiently accurate for most atmospheric radiative transfer applications. Since the absorption coefficients may be taken to be correlated for any pressure and temperature, the correlated k -distribution procedure can be calculated through a nonhomogeneous atmosphere in the same manner as a monochromatic calculation. Thus, the correlated k -distribution allows for an efficient and accurate calculation which is compatible with most multiple scattering routines.

So far, the only information which has been discarded is the precise spectral location of the k values. Nevertheless, transforming the k -distribution from ω space to g space results in an increase in the computational efficiency which is dependent upon the resolution chosen for g space. For calculations involving tropospheric and stratospheric pressure, it has been noted⁹ that the resolution in g space should be of order 0.001 so that the sharply peaked relation between k and g is resolved [see Fig. 1(b)]. Fu and Liou⁹ have found, however, that the sharply peaked k -distribution tends to be confined to the upper 5% of g space, and that a resolution of 0.01 should prove satisfactory for the remainder of g space ($0.0 < g \leq 0.95$). Thus, Fu and Liou⁹ utilized 145 intervals in g space for each $\Delta\omega$ interval. To gain some appreciation of the computational gain, take as an example the spectral interval presented in Fig. 1. To obtain the water vapor absorption spectrum in Fig. 1(a), a line-by-line calculation was performed at a resolution of 0.005 cm^{-1} , which over this 180 cm^{-1} spectral interval yielded 36,000 k 's. Using the g space resolution suggested by Fu and Liou⁹ produced nearly a factor of 250 gain in computational speed, and this example neglects the time taken to compute the k values in the line-by-line calculation.

While significant, an increase in computational speed of two to three orders of magnitude over the line-by-line procedure is still insufficient for production calculations. In addition, further arbitrary reductions in the g space resolution may compromise the accuracy of the calculation. It is therefore necessary to devise a procedure whereby the optimal number of k values can be obtained for a specified accuracy. This optimization, known as the exponential-sum fitting of transmissions (ESFT), was first applied by Hunt and Grant³³ to examine infrared absorbing-scattering problems involving cirrus clouds. The ESFT method has subsequently been utilized for calculations involving clear-skies,^{8, 11, 28, 30, 34-36} cloudy-skies^{11, 28, 37, 38} and aerosol-laden atmospheres.³⁹⁻⁴¹ In the ESFT method, the spectral-mean transmission from Eqs. (4) and (8) are replaced by a fit to a sum of exponentials:

$$T_{\Delta\omega}(u, p, \theta) \simeq \sum_{i=1}^n w_i \exp[-k_i(p, \theta)u]. \quad (9)$$

Thus, $T_{\Delta\omega}(u, p, \theta)$ is approximated by a summation over N monochromatic calculations corresponding to the absorption coefficients $k_i(p, \theta)$ and weights w_i . The physical interpretation of the terms $k_i(p, \theta)$ and w_i leads to the requirements: $k_i(p, \theta) \geq 0$ and $w_i > 0$. In addition, since the transmission function must asymptote to 1 as the molecular abundance approaches 0, a further constraint which must be met is:

$$\sum_{i=1}^N w_i = 1. \quad (10)$$

While extremely useful, exponential-sum fitting is also a classically ill-conditioned problem in numerical analysis.⁴² Wiscombe and Evans⁴³ presented a very comprehensive review and critique

of the available ESFT techniques. They noted that while several approaches had been proposed, each had limitations. To overcome these limitations, Wiscombe and Evans⁴³ developed an elaborate ESFT procedure which masters the ill-conditioning, finds the optimal set of $k_i(p, \theta)$ and w_i , and guarantees to yield the best least-square fit. Yet this procedure has not been a panacea. First, the optimal fit to the transmission function is for equally spaced absorber abundances. Thus, their ESFT function may not necessarily produce accurate transmissions over the required range of absorber abundances (most notably for very low abundances). Second, the strongest argument in favor of the Wiscombe and Evans⁴³ method has been its ability to provide fits with very high accuracies (much better than 0.1%). Nevertheless, Goody et al¹² have noted that the precision to which the radiative properties of molecular species are known may not be sufficient to justify numerical fits with accuracies better than about 1%. Insufficient accuracies in the ESFT functions, however, may produce significant errors in the heating rates.^{35,43} This is the result of the derivative of the transmission function being typically fit at least an order of magnitude worse than the transmission function itself. Thus, less sophisticated ESFT routines than Wiscombe and Evans⁴³ may prove fruitful, but care must be exercised. Finally, the Wiscombe and Evans⁴³ ESFT routines have not been readily available until very recently (June 1994),⁴⁴ and there still remains a question of whether these routines can yield superior fits when employed on typically available computers presently in service.

Considering the unavailability of the Wiscombe and Evans⁴³ ESFT routines when this project was initiated, as well as the need to fit the transmission functions over very wide ranges of abundances, an ESFT method was selected which was similar to the one presented by Chou et al.⁸ Specifically, the values of $k_i(p, \theta)$ are selected *a priori* in such a manner that at the reference pressure and temperature:

$$k_i(p_r, \theta_r) = n k_{i-1}(p_r, \theta_r), \quad (11)$$

where n is a positive integer, and p_r and θ_r represent the reference pressure and temperature. Thus, each of the exponential terms can be derived from the first $k_i(p, \theta)$. This method has proven to be very convenient for constructing the $k_i(p, \theta)$ coefficients for the correlated k -distributions. In addition, it allows for a significant increase in computational speed when a k -distribution is used in conjunction with one-parameter scaling.⁸ Thus, the present method retains the flexibility to be switched from a correlated k -distribution to a k -distribution with a one-parameter scaling if required by computational pressures, and if errors associated with one-parameter scaling are deemed acceptable. Such instances occur with regularity,⁸ however, as previously noted, universal application of the k -distribution technique in association with one-parameter scaling is not justified.^{9,10} It should be noted that enhancement to the computational speed in the k -distribution method reported in Ref. 8 is unavailable for use in the correlated k -distribution method, the reason being that the differences in the pressure and temperature dependences among the $k_i(p, \theta)$'s (see, e.g. Fig. 4 of Ref. 9) are explicitly taken into account, and thus the relationship given by Eq. (11) remains valid only at the reference pressure and temperature.

By utilizing the ESFT method to construct the k -distributions for use by the correlated k -distribution, the number of coefficients is reduced to a level whereby sufficient computational efficiency is obtained to warrant utilization in production calculations. The errors which are incurred by the use of the present method arise from both the deviations from the assumption of correlation and from the accuracy of the ESFT fits. These well-understood errors can be constrained within tolerable limits by a judicious handling of the models.

4. CONSTRUCTION OF THE CORRELATED k -DISTRIBUTIONS FOR AVHRR CHANNELS 1-5

In order to properly interpret the retrieved satellite radiances, it is necessary to understand the radiative processes of the surface-atmosphere system. An inaccurate accounting of any one of these processes could lead to a misinterpretation of the satellite data, with the resultant fallacious assignment of a measurement to the wrong process. The focus of the present study is upon the radiative effects of molecular absorption on top-of-the-atmosphere measured radiances by the AVHRR instruments of the National Oceanic and Atmospheric Administration (NOAA) satellites.

While molecular absorption has been taken into account by several studies of satellite data (see e.g., Refs. 45 and 46), the procedures that were utilized tended to be adapted from climate study models rather than being constructed for the principal purpose of retrieving satellite radiances. The result of such an adaptation is that the derived absorptances may not be representative of the atmospheric absorption occurring within the satellite's spectral channel. Moreover, as noted previously, many parameterized models are unable to properly handle the presence of scattering due to cloud particles or aerosols. To address the concern of the potential impact of molecular absorption upon retrieval satellite measured radiances, this study has constructed for the AVHRR spectral channels correlated k -procedures capable of being incorporated into multiple scattering routines.

The spectral intervals for the AVHRR channels along with their respective average response functions are presented in Table 1. Derived from the NOAA Polar Orbiter data Users Guide,⁴⁷ the information in Table 1 provides an overview of the significant absorbers in each of the AVHRR

Table 1. Spectral intervals taken under consideration. The first column is the subinterval identification number for cross referencing with Fig. 3, the second column is the corresponding AVHRR channel (numbers in parentheses refer to subdivisions in the AVHRR channels), the third and fourth columns define the starting (ω_0) and ending (ω_f) wavenumbers, the fifth column identifies the molecular species included, the sixth column gives the number of k values used for each molecular species, and the seventh column gives the square-wave response function used in conjunction with the correlated k -procedure. Note that subinterval No. 12 has two response functions, the first is for use with AVHRR channel 2, while the second is for use with AVHRR channel 1.

Subinterval #	Channel	ω_0	ω_f	Gas	# of k 's	R
1	AVHRR-5	800	880	H ₂ O	5	0.77426
2	AVHRR-4	880	970	H ₂ O CO ₂	5 2	0.85858
3	AVHRR-3(1)	2490	2560	H ₂ O CH ₄	2 2	0.24603
4	AVHRR-3(2)	2560	2630	H ₂ O CH ₄	2 2	0.97803
5	AVHRR-3(3)	2630	2705	H ₂ O CH ₄	2 2	0.96178
6	AVHRR-3(4)	2705	2775	H ₂ O CH ₄	2 2	0.96992
7	AVHRR-3(5)	2775	2860	H ₂ O CH ₄	2 2	0.62487
8	AVHRR-2(1)	9600	10200	H ₂ O	4	0.20102
9	AVHRR-2(2)	10200	11000	H ₂ O	5	0.64054
10	AVHRR-2(3)	11000	12900	H ₂ O O ₃	6 1	0.80337
11	AVHRR-2(4)	12900	13300	O ₃ O ₂	1 5	0.98912
12	AVHRR-2(5) AVHRR-1(1)	13300	14500	H ₂ O O ₃ O ₂	4 1 3	0.44552 0.24758
13	AVHRR-1(2)	14500	16000	H ₂ O O ₃ O ₂	3 1 3	0.96461
14	AVHRR-1(3)	16000	16600	O ₃	1	0.89060
15	AVHRR-1(4)	16600	17300	H ₂ O O ₃	3 1	0.78896
16	AVHRR-1(5)	17300	17800	H ₂ O O ₃	2 1	0.34804
17		17800	18200	O ₃	1	
18		18200	19200	H ₂ O O ₃	1 1	

Table 2. Comparison of calculations from the correlated k -distribution to the line-by-line procedure for the reduction in the radiative flux from its source (the surface for the thermal infrared and the incoming solar radiation at the top of the atmosphere for the solar) to the top of the atmosphere $\Delta F^{\uparrow}(70)$, the upward radiative flux at the top of the atmosphere $F^{\uparrow}(70)$, the downward radiative flux at the surface $F^{\downarrow}(0)$, and the upward radiative flux at the surface $F^{\uparrow}(0)$ for the thermal infrared cases or the incoming radiative flux at the top of the atmosphere $F^{\downarrow}(70)$ for the solar cases. The top of the atmosphere was taken to be 70 km, and the flux units are in W/m^2 . The fluxes are taken to be positive in the direction of increasing altitude. The three atmospheric cases are the McClatchey et al⁵³ tropical (TRO), midlatitude summer (MLS) and subarctic winter (SAW) atmospheres.

Channel	Atmosphere	Model	$\Delta F^{\uparrow}(70)$	$F^{\uparrow}(70)$	$F^{\downarrow}(0)$	$F^{\uparrow}(0)$
AVHRR-5 (night)	TRO	Line-by-Line	3.4151	28.7134	-22.0760	32.1284
		correlated k	3.4168	28.7286	-22.0605	32.1453
	MLS	Line-by-Line	1.8523	27.6999	-15.5208	29.5522
		correlated k	1.8523	27.7136	-15.4776	29.5659
	SAW	Line-by-Line	0.0454	16.2250	-0.9292	16.2704
		correlated k	0.0448	16.2234	-0.9225	16.2682
AVHRR-4 (night)	TRO	Line-by-Line	2.8313	29.0921	-17.8694	31.9235
		correlated k	2.8276	29.1015	-17.7703	31.9291
	MLS	Line-by-Line	1.4755	27.6574	-11.7369	29.1329
		correlated k	1.4735	27.6616	-11.6549	29.1351
	SAW	Line-by-Line	0.0559	15.0920	-0.6218	15.1479
		correlated k	0.0555	15.0797	-0.6263	15.1352
AVHRR-3 (night)	TRO	Line-by-Line	0.0695	0.6948	-0.1035	0.7645
		correlated k	0.0701	0.6920	-0.1037	0.7622
	MLS	Line-by-Line	0.0410	0.5497	-0.0688	0.5907
		correlated k	0.0414	0.5475	-0.0687	0.5889
	SAW	Line-by-Line	0.0019	0.0913	-0.0040	0.0932
		correlated k	0.0019	0.0908	-0.0039	0.0927
Channel	Atmosphere	Model	$\Delta F^{\uparrow}(70)$	$F^{\uparrow}(70)$	$F^{\downarrow}(0)$	$F^{\downarrow}(70)$
AVHRR-3 (day)	TRO	Line-by-Line	0.1829	0.8804	-2.9314	-3.7520
		correlated k	0.1863	0.8749	-2.9221	-3.7519
	MLS	Line-by-Line	0.1431	0.7637	-3.0419	-3.7520
		correlated k	0.1451	0.7601	-3.0360	-3.7519
	SAW	Line-by-Line	0.0523	0.4068	-3.4518	-3.7520
		correlated k	0.0528	0.4058	-3.4478	-3.7519
AVHRR-2 (day)	TRO	Line-by-Line	5.4148	16.2391	-175.6926	-216.5386
		correlated k	5.4744	16.2078	-175.8564	-216.8221
	MLS	Line-by-Line	4.8030	16.8509	-180.9528	-216.5386
		correlated k	4.8243	16.8579	-181.1416	-216.8221
	SAW	Line-by-Line	2.2881	19.3658	-200.9942	-216.5386
		correlated k	2.2765	19.4057	-201.3543	-216.8221
AVHRR-1 (day)	TRO	Line-by-Line	2.6288	14.7479	-157.7717	-173.7673
		correlated k	2.6369	14.7474	-157.8545	-173.8432
	MLS	Line-by-Line	2.6227	14.7540	-158.2661	-173.7673
		correlated k	2.6211	14.7632	-158.3781	-173.8432
	SAW	Line-by-Line	2.3856	14.9911	-160.5750	-173.7673
		correlated k	2.3786	15.0057	-160.6840	-173.8432

channels. The subdivision of AVHRR channels 1, 2, and 3 into smaller spectral regions is necessitated by the considerable spectral extent of these channels. These AVHRR channels are sufficiently wide that (a) the assumption of constancy for the Planck function over the interval is not appropriate, and (b) the distribution of absorption features attributed to the various molecular species is far from uniform over these intervals. While Planck-weighting⁸ can somewhat ameliorate the former complication, it is not so easy to dismiss the latter complication which arises both from the band shape beginning to contribute significantly to the k -distribution, and from the nonuniformity of the overlap of absorption features of different molecules. In concert with these complications resides a further challenge; the spectral response functions of the satellite instruments are sufficiently complex that utilizing a square-wave function for an entire AVHRR channel may result in significant discrepancies. Thus, the molecular absorption curves and the spectral response functions have been utilized together to determine the selection of the subdivisions for AVHRR channels 1, 2 and 3 (see Table 1). A byproduct of subdividing AVHRR channels 1 and 2 is the ability of the present parameterizations to accommodate the molecular absorption found in other satellite channels such as the Geostationary Operational Environmental Satellite (GOES) visible

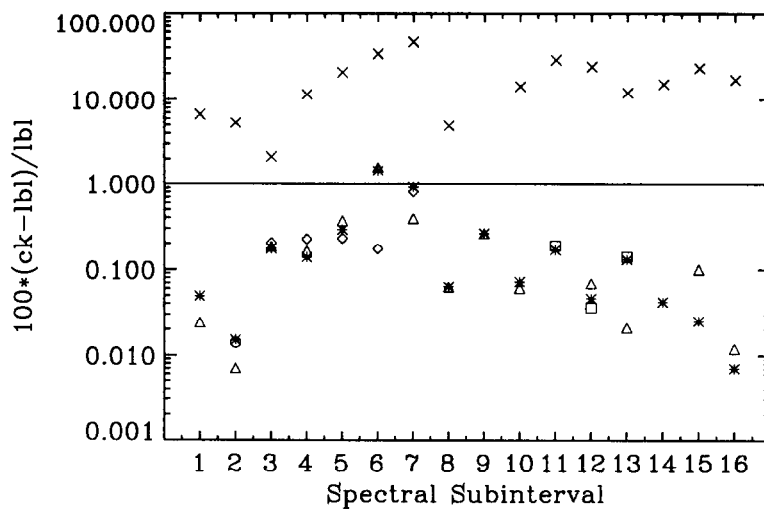


Fig. 2. Absolute values of the percentage errors encountered in the calculation of the outgoing fluxes at the top of the atmosphere by the correlated k -distribution as referenced against the line-by-line procedure for the McClatchey et al.⁵¹ midlatitude summer atmosphere. The comparisons are presented for the molecular species: H_2O (Δ), CO_2 (\circ), CH_4 (\diamond) and O_2 (\square). Comparisons are not presented for O_3 separately, since the O_3 spectrum is not resolved into lines. The influence of incoming solar radiation is taken into consideration for AVHRR channels 3, 4 and 5. Also plotted are the cases where the total of all molecular absorption is included (*), and where molecular absorption is ignored (\times). Note that for subinterval No. 9 the error incurred by ignoring molecular absorption is in excess of 160% and thus falls outside the boundaries of the plot. The subinterval numbers refer to those listed in Table 1.

channel and Landsat channels 2, 3, and 4.⁴⁸ Note, to fully cover the spectral ranges of these satellite channels it was necessary to create parameterizations for two additional subintervals which are presented at the bottom of Table 1.

A summary of the method employed to create the correlated k -distributions is as follows. The line-by-line procedure was run for a specified spectral interval and molecular species at a reference pressure of 500 hPa and a reference temperature of 250 K. The reference pressure and temperature were chosen to be representative of the median value in the troposphere where much of the molecular line absorption occurs in the AVHRR channels. The absorption coefficients produced by the line-by-line procedure were then sorted and binned into cumulative probability space with a resolution of 0.001 (i.e., 1000 intervals). The ESFT technique discussed in Sec. 3 was next used in conjunction with the least-squares procedure of Ref. 49 to obtain optimized fits for a range of abundances extending from 10 times the total atmospheric column abundance down through abundances well into the linear region. By fitting the transmission curves for very large abundances, very long pathlengths can be handled without the concern of extrapolating the k -distribution beyond its realm of applicability. Such very long pathlengths are frequently encountered within scattering routines. The negative side of extending the transmission function fits to very large abundances is that a higher number of k 's are required to obtain a fit to a specified tolerance. It must be noted, however, that a fit which does not encompass anticipated conditions is of limited use. By fitting the transmission curves well into the linear portion of the curve of growth, the constraint given in Eq. (10) can be fulfilled.

With the acquisition of a satisfactory fit for the k -distributions to the line-by-line calculation at the reference pressure and temperature, the next step is to utilize the line-by-line procedure to calculate the absorption coefficients for the spectral interval at some predetermined set of pressures and temperatures which are representative of the atmosphere. The distributions of the k values at these pressures and temperatures are assumed to be correlated with those at the reference pressure and temperature and thus for all atmospheric conditions. Thus, each of the sets of line-by-line generated absorption coefficients can then be sorted and binned with precisely the same distribution as was accomplished for the reference pressure and temperature. For present purposes, the line-by-line calculations were obtained for 19 (11) pressures with $\Delta \log_{10} p = 0.2$ in the thermal infrared (solar), along with three temperatures (210, 250, and 290 K). As demonstrated by Chou

Table 3. Same comparison of calculations from the correlated k -distribution to the line-by-line procedure as presented in Table 2 except that the instrument response function for the AVHRR channels is included in the calculations.

Channel	Atmosphere	Model	$\Delta F^\dagger(70)$	$F^\dagger(70)$	$F^\dagger(0)$	$F^\dagger(0)$
AVHRR-5 (night)	TRO	Line-by-Line	2.6378	22.2398	-17.0517	24.8776
		correlated k	2.6455	22.2434	-17.0805	24.8888
	MLS	Line-by-Line	1.4294	21.4519	-11.9637	22.8812
		correlated k	1.4341	21.4576	-11.9837	22.8917
	SAW	Line-by-Line	0.0361	12.5548	-0.7159	12.5909
		correlated k	0.0347	12.5611	-0.7143	12.5958
AVHRR-4 (night)	TRO	Line-by-Line	2.4248	24.9919	-15.2562	27.4167
		correlated k	2.4277	24.9860	-15.2572	27.4137
	MLS	Line-by-Line	1.2646	23.7491	-10.0023	25.0137
		correlated k	1.2651	23.7497	-10.0067	25.0148
	SAW	Line-by-Line	0.0495	12.9324	-0.5316	12.9820
		correlated k	0.0477	12.9471	-0.5377	12.9948
AVHRR-3 (night)	TRO	Line-by-Line	0.0599	0.4799	-0.0905	0.5397
		correlated k	0.0593	0.4790	-0.0890	0.5383
	MLS	Line-by-Line	0.0352	0.3808	-0.0603	0.4161
		correlated k	0.0349	0.3801	-0.0591	0.4149
	SAW	Line-by-Line	0.0015	0.0629	-0.0034	0.0644
		correlated k	0.0015	0.0627	-0.0033	0.0642
Channel	Atmosphere	Model	$\Delta F^\dagger(70)$	$F^\dagger(70)$	$F^\dagger(0)$	$F^\dagger(0)$
AVHRR-3 (day)	TRO	Line-by-Line	0.1525	0.6164	-2.1551	-2.8317
		correlated k	0.1537	0.6156	-2.1662	-2.8478
	MLS	Line-by-Line	0.1192	0.5385	-2.2442	-2.8317
		correlated k	0.1195	0.5387	-2.2586	-2.8478
	SAW	Line-by-Line	0.0427	0.2984	-2.5854	-2.8317
		correlated k	0.0424	0.3002	-2.6044	-2.8478
AVHRR-2 (day)	TRO	Line-by-Line	3.4954	10.2297	-110.6910	-137.2507
		correlated k	3.5401	10.1850	-110.5443	-137.2505
	MLS	Line-by-Line	3.1173	10.6078	-113.9698	-137.2507
		correlated k	3.1391	10.5860	-113.8248	-137.2505
	SAW	Line-by-Line	1.5415	12.1836	-126.5772	-137.2507
		correlated k	1.5441	12.1810	-126.5488	-137.2505
AVHRR-1 (day)	TRO	Line-by-Line	1.4863	9.9986	-106.2267	-114.8494
		correlated k	1.5080	9.9770	-106.0462	-114.8498
	MLS	Line-by-Line	1.5672	9.9177	-105.9362	-114.8494
		correlated k	1.5843	9.9007	-105.7828	-114.8498
	SAW	Line-by-Line	1.6824	9.8025	-105.5713	-114.8494
		correlated k	1.6888	9.7962	-105.5150	-114.8498

and Kouvaris,¹⁷ a choice of $\Delta \log_{10} p = 0.2$ for the pressure levels results in negligibly small errors in the calculation of spectrally averaged absorption coefficients when used in conjunction with the linear interpolation of pressures given by:

$$k(p) = k_1 + (k_2 - k_1)(p - p_1)/(p_2 - p_1), \quad (12)$$

where k_1 and k_2 are the k values precomputed at pressures p_1 and p_2 , respectively. As suggested by Rodgers and Walshaw,⁵ the temperature dependence of the absorption coefficients can be adequately reproduced for the normal range of atmospheric temperatures by a quadratic in $k(\theta)$:

$$k(\theta) = k(250) + a(\theta - 250) + b(\theta - 250)^2, \quad (13)$$

where the parameters a and b have been determined from the k values at temperatures $\theta = 210$, 250 and 290 K. A series of sensitivity calculations indicated that the linear in k quadratic temperature interpolation of Eq. (13) yielded comparable accuracies to the logarithmic in k quadratic temperature interpolation employed by Fu and Liou,⁹ while providing a non-negligible increase in efficiency. Once the correlated k values are calculated for the predetermined set of pressures and temperatures, the interpolation schemes can then be utilized to ascertain the coefficient's pressure and temperature dependence.

Frequently, the absorption within a spectral interval arises from a combination of overlapping absorption features from several molecular species. The importance of properly considering the radiative impact of this overlap phenomenon has been well established,⁵⁰ and several techniques^{7,9,10,51} have been devised to account for the overlap of absorption features. The standard

procedure to account for the overlap of the spectral features of different molecular species is to employ the multiplication transmissivity property⁷ which inherently assumes that the spectral features of the different molecular species are uncorrelated with one another. The spectral mean transmittance for the combination of any two different molecular species can thus be expressed in terms of the double summation:

$$T_{\Delta\omega}(u_1, u_2, p, \theta) \simeq \sum_{i=1}^N \sum_{j=1}^M \{w_i \exp[-k_i(p, \theta)u_1]\} \{w_j \exp[-k_j(p, \theta)u_2]\}, \quad (14)$$

where N and M denote the number of correlated k values, and u_1 and u_2 represent the pathlength abundances of the individual molecular species. The use of the multiplication transmissivity property allows for a determination of the transmittance from a combination of the correlated k -distributions of the individual molecular species. This allows for substantial flexibility in regards to changes in the relative abundances of the molecular species. This flexibility, however, is obtained at the cost of performing $N \times M$ spectral calculations for every vertical column required to determine radiative fluxes and heating rates for the spectral intervals where the two molecular species overlap. In order to enhance computational efficiency, Lacis and Oinas¹¹ considered the overlapping absorption bands by combining the absorption parameters into a single Malkmus band model² that was constrained to be accurate in the strong and weak line limits. As noted by Goody et al.,¹² however, except for the strong and weak line limits, the convolution of two Malkmus bands does not constitute a Malkmus band. In addition, employing the Malkmus model to simulate the k -distribution introduces serious limitations which are best avoided.^{12,43} Another method is to consider a correlated k -distribution which is constructed for the combined absorption of the overlapping molecular species.^{9,51} The chief advantage of this method is a significant reduction in the number of spectral calculations. Indeed, for the 540–800 cm^{-1} region, Fu and Liou⁹ obtained a factor of four reduction in computational burden. The drawback to this method is that it is necessary to recalculate the correlated k -distribution every time the relative mixing ratios of the absorbers is altered.¹² Nevertheless, this procedure has many useful applications, especially when computational time is at a premium. For present purposes, however, the flexibility of the multiplication transmissivity property makes that method preferable.

Presented in Table 1 is a summary of the ESFT correlated k -distributions for the molecular absorption occurring within the spectral bounds of the AVHRR channels.

5. ATMOSPHERIC FLUX AND HEATING RATE CALCULATIONS

In order to determine the radiative impact of molecular absorption in the AVHRR channels and to facilitate a comparison of the correlated k -distribution technique to the line-by-line procedure, flux calculations for both the upward and downward fluxes were obtained throughout the atmosphere. A resolution of 1 km was employed from the surface to 25 km, and a resolution of 5 km was employed from the 25 km to the top of the atmosphere, taken to be 70 km. To be compatible with the Intercomparison of Radiation Codes used in Climate Models (ICRCCM),⁵² the present study employed the updated versions of the McClatchey et al.⁵³ atmospheres as reported in Ref. 52. Since the focus of the present work is on the radiative effects of molecular absorption for the clear-sky case, the radiative effects of clouds and aerosol layers will be left for future consideration.

The flux $F_{\Delta\omega}(z)$ for the wavenumber interval $\Delta\omega$ at altitude z is taken to be positive in the direction of increasing altitude and may be written as:

$$F_{\Delta\omega}(z) = \pi B_{\Delta\omega}(\theta_s) T_{\Delta\omega}[z/\mu] + \pi \int_0^z B_{\Delta\omega}(\theta) dT_{\Delta\omega}[(z - z')/\mu] + \pi \int_z^{z_\infty} B_{\Delta\omega}(\theta) dT_{\Delta\omega}[(z' - z)/\mu]. \quad (15)$$

The terms of Eq. (15) not previously defined include the Planck function $B_{\Delta\omega}$, the surface temperature θ_s , the altitude taken for the top of the atmosphere z_∞ , and the cosine of the zenith angle μ . As written, Eq. (15) applies directly to the correlated k -distribution model with $B_{\Delta\omega}$ being evaluated at the band center. For the line-by-line procedure, Eq. (15) is a monochromatic expression which can then be integrated over the spectral interval. Hemispherical averaging is performed using an eight-point Gaussian quadrature.

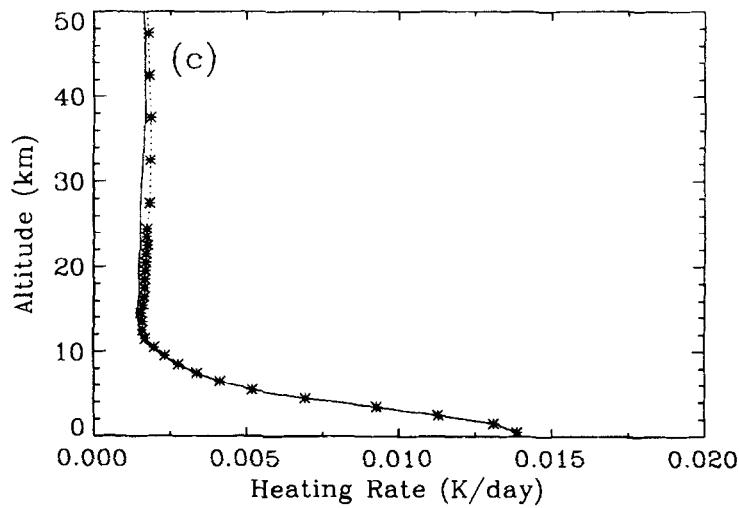
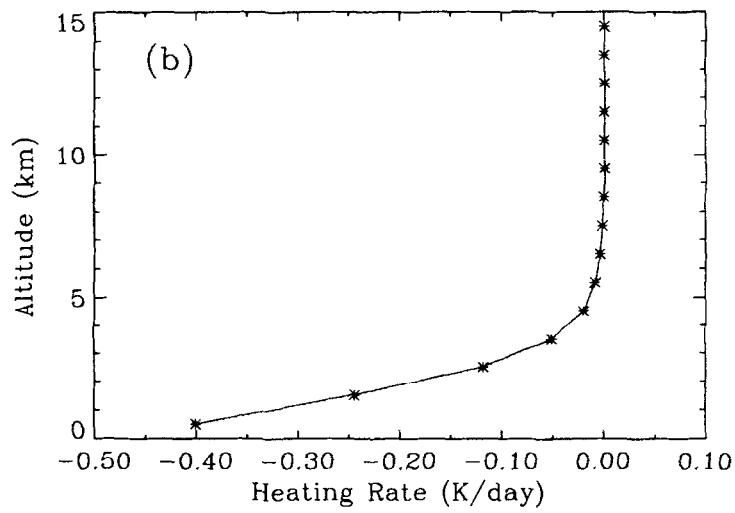
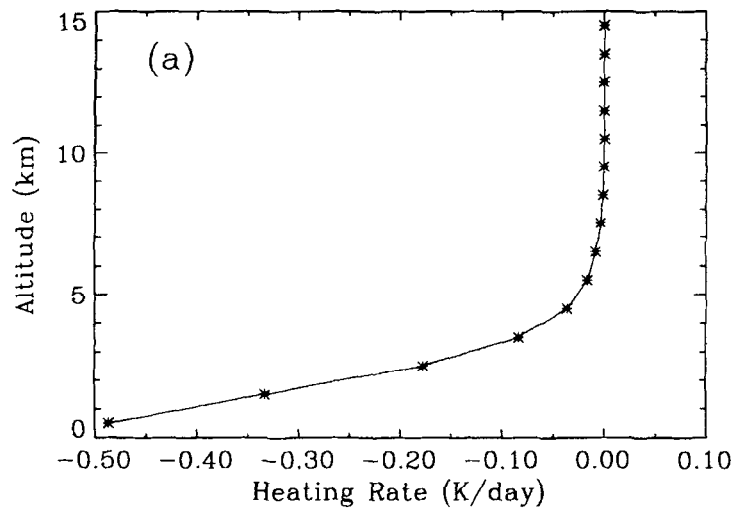


Fig. 3(a)-(c). Continued on opposite page.

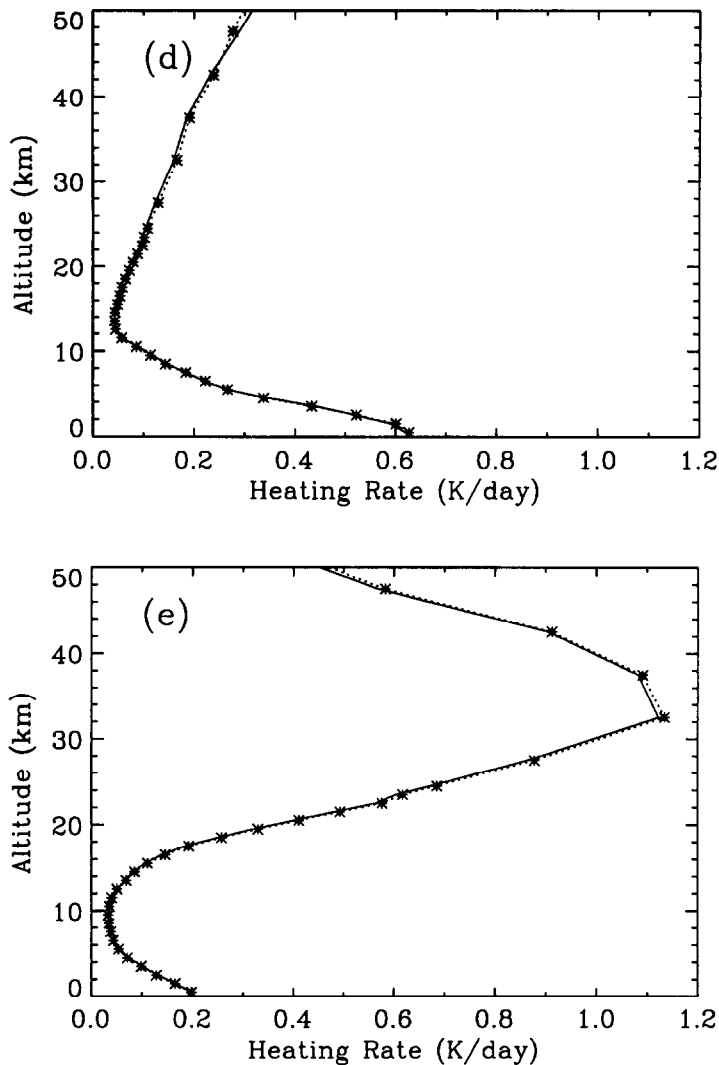


Fig. 3(d) and (e).

Fig. 3. Comparisons of the atmospheric heating rates between line-by-line calculations (solid curves) and correlated k -distribution calculations (dotted curves) for the McClatchey et al.⁵³ midlatitude summer atmosphere. For clarity asterisks have been added to the correlated k -distribution curve. The individual plots represent (a) AVHRR channel 5, (b) AVHRR channel 4, (c) AVHRR channel 3, (d) AVHRR channel 2, (e) AVHRR channel 1. The heating is attributed to H_2O in AVHRR channels 1–5, CO_2 in AVHRR channel 4, CH_4 in AVHRR channel 3, O_2 in AVHRR channels 1 and 2, and O_3 in AVHRR channels 1 and 2.

A comparison of the calculations from the correlated k -distribution to the line-by-line procedure is presented in Table 2 for the reduction in the radiative flux from its source (the surface for the thermal infrared and the incoming solar radiation at the top of the atmosphere for the solar) to the top of the atmosphere $\Delta F^\uparrow(70)$, the upward radiative flux at the top of the atmosphere $F^\uparrow(70)$, the downward radiative flux at the surface $F^\downarrow(0)$, and the upward radiative flux at the surface $F^\uparrow(0)$ for the thermal infrared cases (AVHRR channels, 3, 4, and 5) or the incoming radiative flux at the top $F^\downarrow(70)$ of the atmosphere for the solar cases (AVHRR channels 1, 2, and 3). For the thermal infrared cases (AVHRR channels 4 and 5), the surface is taken to be a perfect emitter. For the solar cases (AVHRR channels 1, 2, and 3), the surface is taken to possess a reflectivity of 10%. The incoming solar radiation is represented by a blackbody of temperature 5710 K (see, e.g., Ref. 54) with a cosine of the solar zenith angle equal to 0.6. Since the spectral location of AVHRR channel 3 is in the proximity of the crossover between the thermal infrared and solar spectra, both the nighttime (infrared) and daytime (infrared plus solar) cases are taken into consideration. In

order to gauge the accuracies of the correlated k -distribution calculations for a wide range of atmospheric conditions, the results in Table 2 are presented for McClatchey et al.⁵³ tropical (TRO), midlatitude summer (MLS), and subarctic winter (SAW) atmospheres. From Table 2 it can be observed that the correlated k -distribution routines yield results which are in excellent agreement with those from the line-by-line procedure. Concentrating for a moment on the upward flux at the top of the atmosphere, which is representative of the energy received by a satellite instrument, it is found that the correlated k -routines yield fluxes within 0.2% of the line-by-line calculation, except for AVHRR channel 3. The slope of the thermal infrared emission curve in the AVHRR channel 3 spectral region is sufficiently steep that the use of an average Planck curve for these subintervals (see Table 1) yields noticeable discrepancies which push the flux error up to about 0.5%. Errors of this magnitude, however, are well within the limits of acceptability. A further examination of Table 2 reveals that the very sensitive integrated flux reductions to the top of the atmosphere as obtained from the correlated k -distribution are in good agreement with those of the line-by-line procedure. The radiative forcing of a particular molecular species is, of course, related to its induced flux reduction at the various levels in the atmosphere, and thus the flux reduction should be accurately calculated (see, e.g., Refs. 55 and 56).

To further illustrate the accuracy of the correlated k -routines, the absolute values of the percentage errors encountered in the calculation of the outgoing top-of-the-atmosphere fluxes by the correlated k -distribution as referenced against the line-by-line procedure are presented in Fig. 2 for the McClatchey et al.⁵³ midlatitude summer atmosphere. From Fig. 2 it is observed that the top-of-the-atmosphere fluxes as calculated by the correlated k -routines are within 1% of those from the line-by-line procedure, except for the subinterval which corresponds to the wavenumber range from 2705 to 2775 cm^{-1} which is error by 1.2%. As noted previously, however, the error associated with the AVHRR channel 3 subintervals is enlarged because of the steepness of the Planck curve. Indeed, except for the AVHRR channel 3 subintervals, the accuracies of the correlated k -routines tend to be of order 0.2% or better. Also presented in Fig. 2 are comparisons of calculations neglecting molecular absorption to reference line-by-line calculations for top-of-the-atmosphere fluxes. By ignoring molecular absorption in the atmosphere, errors of order 10% are regularly encountered. This emphasizes the need to properly account for molecular absorption in the AVHRR channels.

The calculations discussed have so far assumed perfect spectral response functions for the AVHRR satellite instruments. The response functions for these instruments however, are known to be less than perfect and quite complex.⁴⁷ Thus, it is necessary to compare the results of the correlated k -distribution calculations to the line-by-line calculations for the cases where the response functions are taken into account. Such comparisons are presented in Table 3 for conditions identical to those in Table 2 except that the satellite instrument response functions are taken into consideration for both the correlated k -distribution and line-by-line calculations. The response functions utilized in the line-by-line calculations were obtained directly from the spectral response curves reported for the NOAA-12 satellite by Ref. 47, while the square-wave response functions given in Table 1 which were derived from the NOAA-12 response functions, were utilized in the correlated k -distribution calculations. From a perusal of the comparisons presented in Table 3, it is observed that despite the added complexity of the response functions, the accuracies of the correlated k -distribution calculations relative to the line-by-line calculations are very similar to those presented in Table 2. Thus, the incorporation of the response function does not compromise the accuracy of the present correlated k -distributions. Nevertheless, several notes are in order. First, the narrow spectral extent of the absorption due to the A, B, and γ bands of O_2 (see Ref. 57) requires careful handling. This is most notable in the spectral region where AVHRR channels 1 and 2 overlap (subinterval No. 12 of Table 1). In this spectral region, the AVHRR channel 1 response function entirely eliminates the contribution due to O_2 , while the AVHRR channel 2 response function enhances the relative contribution due to O_2 . Second, if not for the AVHRR channel 3 response function, a single correlated k -distribution capable of yielding satisfactory transmissions calculations could be produced for the entire channel. Previously noted errors which would be introduced when utilizing an average Planck function or AVHRR channel 3 could be easily taken into account by a judicious use of Planck-weighting.⁸ Third, while the conclusions drawn here can be relied upon for the AVHRR channels, they should not be extrapolated to other satellite channels without due consideration.

As noted previously, the radiative forcing ascribed to an absorption band of a molecular species can be determined from its induced flux reduction. It is frequently convenient to calculate this radiative forcing in terms of heating rates. The heating rate is the change in temperature $\Delta\theta$ over a specified time interval Δt , and is calculated from the divergence of the net flux ΔF over a pressure interval Δp , and is given by:

$$\frac{\Delta\theta}{\Delta t} = \frac{\mu g}{C_p} \frac{\Delta F_{\Delta\omega}}{\Delta p}, \quad (16)$$

where μ is the cosine of the zenith angle, g is the gravitational acceleration, and c_p is the specific heat at constant pressure. Because the heating rates are related to the derivative of the fluxes, and hence to the derivative of the transmission functions, they are very sensitive to small errors in the fluxes. Thus, heating rates not only provide information on where absorption occurs in the atmosphere, but they also provide a very sensitive mechanism for determining the accuracy of a parameterized model. Heating rate calculations as obtained from the correlated k -distribution techniques as well as the line-by-line procedure are presented in Fig. 3 for the molecular absorption present in AVHRR channels 1–5. The results of these heating rate calculations for the McClatchey et al⁵³ midlatitude summer atmosphere clearly demonstrate the ability of the present correlated k -routines to accurately simulate the absorption calculated by the line-by-line procedure.

Heating rates for AVHRR channels 5 and 4 are presented in Fig. 3(a) and (b) respectively, for the altitude range from 0 to 15 km. The heating rates in both of these nighttime (infrared only) cases are dominated by the absorption due to water vapor and are virtually zero for altitudes above 15 km. The weak 10.4 μm CO_2 absorption band involved with AVHRR channel 4 induces only a small alteration to the heating rate presented in Fig. 3(b); however, it has been noted that for regions of the atmosphere undergoing large-scale subsidence this CO_2 absorption might allow for remote detection of marine stratus clouds.⁵⁸ Heating rates for AVHRR channels 3, 2, and 1 are presented in Figs. 3(c)–(e), respectively, for the altitude range from 0 to 50 km. The heating rate profiles in these three daytime (infrared plus solar) cases are complex combinations of constituent molecular species. To avoid confusion, only the combined heating rates from all the involved molecular species are plotted in Fig. 3, i.e., the heating rates for the individual gases are not plotted. A quick summary of the contributions from the individual molecular species is as follows. The heating rate for the spectral range corresponding to AVHRR channel 3 [Fig. 3(c)] is dominated by H_2O below 8 km and by CH_4 above 8 km. For AVHRR channel 2 [Fig. 3(d)], the heating rate is dominated by H_2O below 10 km, by O_3 between 20 and 40 km, and by O_2 between 10 and 20 km and above 40 km. For AVHRR channel 1 [Fig. 3(e)], the heating rate is dominated by H_2O below 9 km and O_3 above 9 km.

A final notable result is a discrepancy in the heating rates for the A, B, and γ bands of O_2 as calculated by the present models and as reported in Fig. 2 of Ref. 59. Specifically, Kiehl and Yamanouchi⁵⁹ find that the heating rates attributable to O_2 are around 0.26 K/day throughout the altitude range from 20 to 50 km. The present calculations yield comparable results below 30 km (heating rates vary from 0.27 to 0.33 K/day in the stratosphere below 30 km); however, the present calculations also yield rapidly rising heating rates above 30 km. Indeed, at an altitude of 50 km the present calculations indicate that the heating rate is an order of magnitude greater than that reported in Ref. 59. In an attempt to resolve the situation, further comparisons were made to the differential flux calculations reported by Chou.⁶⁰ The agreement between the present line-by-line calculations and those reported in Ref. 60 is quite good; however, the altitude resolution provided in Ref. 60 is not sufficient to make a conclusive appraisal.

6. SUMMARY

An ESFT technique was applied to line-by-line absorptance calculations to produce correlated k -distributions for the five AVHRR spectral channels. To determine the accuracy of the correlated k -distribution routines, atmospheric flux and heating rate calculations were run against reference line-by-line calculations for a wide variety of atmospheric conditions. For the atmospheric conditions taken into consideration, the correlated k -distribution routines yielded highly satisfactory results for both the cases where the satellite spectral response functions were and were not

applied. The principal advantage of the correlated k -distribution technique is that it can be incorporated directly into multiple scattering routines that consider scattering and absorption by clouds and aerosol particles. Thus, as noted by Goody et al¹² the correlated k -distribution can be employed in iterative methods involved with the inversion of satellite radiances or in numerical weather or climate models. The routines utilizing these correlated k -distributions for the AVHRR bands are available from the author by request.

Acknowledgements—The author would like to acknowledge the numerous beneficial discussions with B. A. Wielicki. This work was supported by funding from the NASA Earth Observing System program.

REFERENCES

1. R. M. Goody, *Quart. J. R. Meteor. Soc.* **78**, 165 (1952).
2. W. Malkmus, *J. Opt. Soc. Am.* **57**, 323 (1967).
3. V. Ramanathan, *J. Atmos. Sci.* **33**, 1330 (1976).
4. M.-D. Chou, D. P. Kratz, and W. Ridgway, *J. Climate* **4**, 424 (1991).
5. C. D. Rodgers and C. D. Walshaw, *Quart. J. R. Meteor. Soc.* **92**, 67 (1966).
6. K.-N. Liou, *An Introduction to Atmospheric Radiation*, Academic Press, New York (1980).
7. R. M. Goody and Y. L. Yung, *Atmospheric Radiation, Theoretical Basis*, pp. 127, 128, 208, 223–236. Oxford University Press, New York (1989).
8. M.-D. Chou, W. L. Ridgway, and M. M.-H. Yan, *J. Atmos. Sci.* **50**, 2294 (1993).
9. Q. Fu and K. N. Liou, *J. Atmos. Sci.* **49**, 2139 (1992).
10. A. A. Lacis, W. C. Wang, and J. Hansen, *NASA Conf. Publ.*, 2076, pp. 309–314 (1979).
11. A. A. Lacis and V. Oinas *J. Geophys. Res.* **96**, 9027 (1991).
12. R. Goody, R. West, L. Chen, and D. Crisp, *JQSRT* **42**, 539 (1989).
13. L. S. Rothman, R. R. Gamache, R. H. Tipping, C. P. Rinsland, M. A. H. Smith, D. C. Benner, V. M. Devi, J.-M. Flaud, C. Camy-Peyret, A. Perrin, A. Goldman, S. T. Massie, L. R. Brown, and R. A. Toth. *JQSRT* **48**, 469 (1992).
14. F. Schreier, *JQSRT* **48**, 743 (1992).
15. J. Humlíček, *JQSRT* **27**, 437 (1982).
16. S. B. Fels and M. D. Schwarzkopf, *J. Geophys. Res.* **86**, 1205 (1981).
17. M.-D. Chou and L. Kouvaris, *J. Geophys. Res.* **91**, 4047 (1986).
18. M.-D. Chou, *J. Climate Appl. Metreor.* **25**, 1532 (1986).
19. P. Varanasi, *JQSRT* **40**, 169 (1988).
20. W. B. Grant, *Appl. Opt.* **29**, 451 (1990).
21. R. E. Roberts, J. E. A. Selby, and L. M. Biberman, *Appl. Opt.* **15**, 2085 (1976).
22. J. T. Kiehl and V. Ramanathan, *J. Atmos. Sci.* **39**, 2923 (1982).
23. W. L. Ridgway, Harshvarden, and A. Arking, *J. Geophys. Res.* **96**, 8969 (1991).
24. E. C. Y. Inn and Y. Tanaka, *J. Opt. Soc. Am.* **43**, 870 (1953).
25. *Atmospheric Ozone 1985*, WMO Global Ozone Reserch Monitoring Project, Report No. 16, I. Chap. 7 (1986).
26. J. T. Houghton, *The Physics of the Atmospheres*, pp. 178–179, Cambridge University Press, New York (1979).
27. S. S. Penner, *Quantitative Molecular Spectroscopy and Gas Emissivities*, p. 74, Addison-Wesley, Reading, MA (1959).
28. A. A. Lacis and J. E. Hansen, *J. Atmos. Sci.* **31**, 118 (1974).
29. V. Ambartzumian, *Publ. Obs. Astron. Univ. Leningrad.* **6**, 7 (1936).
30. A. Arking and K. Grossman, *J. Atmos. Sci.* **29**, 937 (1972).
31. M.-D. Chou and A. Arking, *J. Atmos. Sci.* **37**, 855 (1980).
32. W.-C. Wang and G.-Y. Shi, *JQSRT* **39**, 387 (1988).
33. G. Hunt and I. Grant, *J. Atmos. Sci.* **26**, 963 (1969).
34. M.-D. Chou and A. Arking, *J. Atmos. Sci.* **38**, 798 (1981).
35. S. Asano and A. Uchiyama, *JQSRT* **38**, 147 (1987).
36. A. S. Grossman and K. E. Grant, *Proc. 8th Conf. Atmospheric Radiation*, pp. 97–99, Nashville, TN (1994).
37. G. Yamamoto, M. Tanaka, and A. Asano, *JQSRT* **11**, 697 (1971).
38. S. Sargent and W. Beckman, *J. Atmos. Sci.* **30**, 88 (1973).
39. K. Liou and T. Sasamori, *J. Atmos. Sci.* **32**, 2166 (1975).
40. J. Pollack, O. Toon, A. Summers, W. Van Camp, and B. Baldwin, *J. Appl. Metreor.* **15**, 247 (1976).
41. G. L. Stephens, *J. Atmos. Sci.* **35**, 2111 (1978).
42. F. S. Acton, *Numerical Methods that Work*, p. 541, Harper & Row, New York (1970).
43. W. J. Wiscombe and J. W. Evns, *J. Comp. Phys.* **24**, 416 (1977).
44. W. J. Wiscombe, private communication (1994).
45. B. P. Brieglieb, P. Minnis, V. Ramanathan, and E. Harrison, *J. Climate Appl. Metreor.* **25**, 214 (1986).
46. B. A. Baum, R. F. Arduini, B. A. Wielicki, P. Minnis, and S.-C. Tsay, *J. Geophys. Res.* **99**, 5499 (1994).

47. K. B. Kidwell, *NOAA Polar Orbiter Data Users Guide*, p. 280, NOAA, Washington, DC (1991).
48. E. Schmidt, private communication (1994).
49. W. H. Press, B. P. Flannery, S. A. Teukolsky, and W. T. Vetterling, *Numerical Recipes*, Chap. 14, Cambridge University Press, New York (1986).
50. W.-C. Wang and P. B. Ryan, *Tellus* **35B**, 81 (1983).
51. M. F. Gerstell, *JQSRT* **49**, 15 (1993).
52. R. G. Ellingson, J. Ellis, and S. Fels, *J. Geophys. Res.* **96**, 8929 (1991).
53. R. A. McClatchey, R. W. Fenn, J. E. Selby, F. E. Volz, and J. S. Garing, *Optical Properties of the Atmosphere*, 3rd edn. AFCRL-72-0497, Environmental Research Papers No. 411 (1972).
54. J. W. Chamberlain, *Theory of Planetary Atmospheres*, p. 330, Academic Press, New York (1978).
55. D. P. Kratz, B.-C. Gao, and J. T. Kiehl, *J. Geophys. Res.* **96**, 245 (1991).
56. D. P. Kratz and P. Varanasi, *JQSRT* **48**, 245 (1992).
57. T. Nakazawa, T. Yamanouchi, and M. Tanaka, *JQSRT* **27**, 615 (1982).
58. C. Prabhakara, J.-M. Yoo, D. P. Kratz, and G. Dalu, *JQSRT* **49**, 599 (1993).
59. J. T. Kiehl and T. Yamanouchi, *Tellus* **37B**, 1 (1985).
60. M.-D. Chou, *J. Climate* **3**, 209 (1990).